Nanoscale

Accepted Manuscript

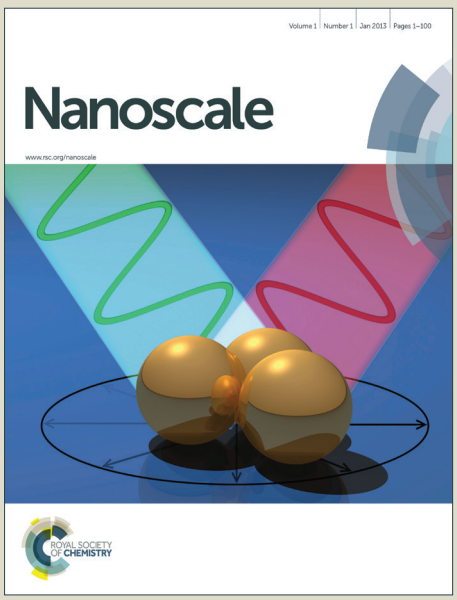

ROYAL SOCIETY OF CHEMISTRY

www.rsc.org/nanoscale

Journal Name

RSCPublishing

ARTICLE

Nanocomposites of AgInZnS and Graphene nanosheets as Efficient Photocatalysts for Hydrogen Evolution

Cite this: DOI: 10.1039/x0xx00000x

Xiaosheng Tang[1*], Weiwei Chen[1], Zhiqiang Zu[1], Zhigang Zang[1*], Ming Deng[1], Tao Zhu[1], Kuan Sun[2], Lidong Sun[3], Junmin Xue[4]

Received 00th January 2012,
Accepted 00th January 2012

DOI: 10.1039/x0xx00000x

www.rsc.org/

In this study, AgInZnS-reduced graphene（AIZS-rGO） nanocomposites with with tunable band gap absorption and large specific surface area were synthesized by a simple hydrothermal route, which showed high efficient photocatalytic hydrogen evolution under visible-light irradiation. The relationships between crystal structure, morphology, surface chemical states and photocatalytic activity have been explored in detail**.** Importantly, the AIZS-rGO nanocomposites with 0.02 wt% of graphene exhibited the highest hydrogen production rate of 1.871 mmol $h^{-1}g^{-1}$, which was nearly 2 times the hydrogen production rate by using pure AIZS nanoparticles as the photocatalyst. This high photocatalytic H_2-production activity was attributed predominantly to the incorporation of graphene sheets, which demonstrated an obvious influence on the structure and optical properties of the AIZS nanoparticles. In the AIZS-rGO nanocomposites, the graphene could not only serve as an effective supporting layer and also is a recombination center for conduction band electrons and valence band holes. It is believed that this kind of graphene-based materials would attract much attention as a promising photocatalyst with high efficiency and low cost for photocatalytic H_2 evolution and facilitates their applications in the environmental protection field.

.

Introduction

In order to moderate the reliance on exhaustible natural resources and the environmental contamination which caused by combustion of fossil fuels, a large number of scientists are searching for low cost renewable energy conversion materials.[1-4] Photocatalytic hydrogen evolution from water splitting using semiconductor photocatalysts has been considered as one of the most important methods to solve the energy crisis, since the Honda's group reported that the hydrogen could be produced through the photoelectron chemical splitting of water on TiO_2 electrodes.[4-7] In the past several years, large numbers of photocatalysts materials are reported to have high photocatalytic activity for water splitting under UV light. However, UV light only accounts for 4% of the incoming solar energy, whereas the visible light is 43%.[4, 7] Therefore, lots of research groups are searching the semiconductor materials which could be prepared as photocatalysts for water splitting to hydrogen under visible-light irradiation. In recent years, a large numbers of phtocatalyts have been synthesized; however, only few effective photocatalysts for hydrogen evolution under visible-light irradiation have been reported. Kudo and Chen's group studied sulfide-based solid solutions respectively, such as ZnS-$AgInS_2$,[8, 9] ZnS-$CuInS_2$[10, 11] and ZnS-$AgInS_2$-$CuInS_2$,[12] they have been extensively studied because of their controllable band structures and excellent performance for photocatalytic hydrogen production under visible light irradiation. However, the high-temperature heat treatment or the toxicity solvents are needed for preparing these solid solutions respectively.[9, 10, 13] Thus，developing a facile and environmental friendly method to synthesize semiconductor materials for achieving high efficient hydrogen production is still a challenge.

Graphene, a two dimensional carbonaceous material which can be used in many applications such as catalytic, optical, battery, because of its unique properties of high conductivity,

excellent mobility of charge carriers and the large specific surface area. Up to now, lots of methods have been reported for the synthesis of graphene, including micromechanical cleavage, thermal exfoliation, and electrochemical reduction of graphite oxide. Among these methods, the reduction of exfoliated graphene oxide was proved to be an effective approach to achieve graphene nanosheets.[14-18] Recently, it has been reported graphene oxide (GO) or reduced graphene oxide (rGO)-based semiconductor could be an efficient co-catalyst for photocatalytic hydrogen production due to their good electron conductivity, large specific surface area and high adsorption.[19, 20] Cui *et al.* evaluated the photocatalytic performance of a graphene/TiO_2 nanocomposites, and the study demonstrated that the hydrogen production rate of graphene based nanocomposites could increase to 8.6 μmol h^{-1}, the productivity is nearly about twice compared to pure commercial TiO_2 catalyst. [21] However, most of hydrogen production rate of the graphene based composites is not outstanding under visible light; moreover, some of them contain toxic elements such as Pb or Cd, which would lead to environmental pollution. Therefore, it is still necessary to develop an environmental friendly method for synthesizing graphene based nanocomposits for phtotocatalytic hydrogen production under visible light.

Herein, AIZS-rGO nanocomposites with high efficiency photocatalytic hydrogen production rate under visible-light were achieved using hydrothermal method. The as-obtained AIZS-rGO nanocomposites reached high hydrogen production rate of 1.871 mmol h^{-1} g^{-1} which is about 2 times of pure AIZS nanospheres (0.951 h^{-1} g^{-1}). This high photocatalytic of hydrogen production rate arises from the presence of graphene, which could serve as an electron collector and transporter to efficiently lengthen the lifetime of photogenerated charge carriers from AIZS nanospheres and it also could effectively inhibit the recombination of electron-hole pairs in the AIZS-rGO composites. Furthermore; the successfully prepared AIZS-rGO nanocomposites provide of an effective approach to synthesize graphene-based composites in the field of energy conversion.

Experimental Section

Preparation of photocatalysts

AIZS photocatalysts were prepared *via* a hydrothermal method. In a typical experiment synthesizing sample, $Zn(Ac)_2{\cdot}2H_2O$ (395 mg), $InCl_3{\cdot}4H_2O$ (87.9 mg), $AgNO_3$ (19.3 mg), and excess of thioacetamide (200 mg) were dissolved into 15 mL of distilled water using a magnetic stirrer to form a clear solution. The reaction mixture was immediately transferred into an autoclave (Teflon cups with 50 mL inner volume). The autoclave was maintained at 180 ℃ for 18 h and then air-cooled to room temperature. The product was collected by centrifugation, washed several times with absolute ethanol and finally air dried. Samples with different Ag, In, Zn ratios in the starting materials were prepared under the identical conditions ($Ag_{0.01}In_{0.23}ZnS_{1.35}$, $Ag_{0.02}In_{0.23}ZnS_{1.355}$, $Ag_{0.04}In_{0.23}ZnS_{1.365}$ and $Ag_{0.05}In_{0.23}ZnS_{1.37}$) in order to investigate the role of composition on photocatalytic activities.

Preparation of GO

GO was prepared by oxidation of natural flake graphite powder using a modified Hummers method.[22] In a typical synthesis, 1 g graphite powder and 1 g $NaNO_3$ was mixed, and then put into 46 mL concentrated H_2SO_4 (98%) with a ice bath. After magnetically stirred for one hour, 6 g $KMnO_4$ was gradually added into the mixture under stirring. The mixture was then transferred to a water bath of 35°C for one day. Successively, 40 mL H_2O was slowly added into the mixture, during which the temperature of the mixture rose to approximately 80 °C. Finally, 100 mL H_2O followed by 20 mL 20% H_2O_2 solution was added into the mixture, and the mixture was further stirred for 30 minutes. The final product (GO) was collected by centrifugation, and was repeatedly rinsed with 4% HCl solution followed by de-ionized water. Finally, the oxidized graphite was dried in an oven at 70°C for four days.

Preparation of AIZS-rGO nanocomposites

In a typical synthesis of AIZS-rGO (AG) nanocomposites, the as-prepared GO and the precursors including $Zn(Ac)_2{\cdot}2H_2O$ (395 mg), $InCl_3{\cdot}4H_2O$ (87.9 mg), $AgNO_3$ (19.3 mg), and excess of thioacetamide (200 mg)were dissolved into 15 mL distilled water. The mixture was sonicated for 30 mins. Next, the mixture solution was immediately transferred into an autoclave (Teflon cups with 50 mL inner volume). The autoclave was maintained at 180 °C for 18 h and then air-cooled to room temperature. The product was collected by centrifugation and washed for several times with absolute ethanol and finally dried in air.

Characterization of Photocatalysts

The crystal structures of products were inverstigated by an Advanced Diffractometer System (D8 Advanced Diffractometer System, Bruker, Karlsruhe, Germany). All transmission electron microscopy (TEM) images were obtained using JEOL 3010 microscope at an acceleration voltage of 200 kV. X-ray photoelectron spectroscopy (XPS) was performed with the Phobios 100 electron analyzer equipped with 5 channertrons, using an unmonochromated Al Kα X-ray source (1486.6 eV). The structures of hybrid nanofibers were investigated using an X-ray powder diffractometer (XRD, Bruker D8 Discover) with Cu Kα radiation. UV-Vis absorption spectra were recorded on a UV-1601 Spectrophotometer. BET specific surface areas and pore volumes were calculated from nitrogen adsorption/desorption isotherms determined at 77 K using an AUTO-SORB-1-MP surface analyser (the sample was outgrassed under vacuum at 200 ⍰).

Photocatalytic Reactions

The photocatalytic reaction was performed in a closed gas-circulation system. The reaction cell was made up of Pyrex glass with a quartz window suitable for vertical illumination. A 300 W high pressure Xe lamp (Oriole instruments, USA) was used as a light source. A 420 nm cut-off filter was employed to screen the UV light. The IR component in the radiation was removed by circulating water filter. The air in the reaction cell was removed by purging the argon gas. In all tests, 100 mg of catalyst was suspended in 100 mL of 1.2 M Na_2SO_3 and 0.1 M Na_2S solution by magnetic stirring. The reaction was carried out for different hours and the amout of hydrogen evolved was analyzed by gas chromatograph (Shimazu GC-2014; Molecular sieve 5A, TCD detector, Ar carrier gas).

Results and Discussion

The crystal structures of the synthesiszed AIZS nanospheres were investigated by the X-ray diffraction (XRD). As showed in the Figure 1A, the main diffraction peak positions of the obtained products are 28.6°, 47.6° and 56.5° corresponding to the diffractions of the (111), (220) and (311) planes which can be indexed to ZnS (JCPDS No. 65-0309), confirming the cubic zinc blende structure of the AIZS nanoparticles.[10] It could be observed that the major peaks of the XRD patterns did not change obviously with the ratio of the graphene increasing, this was due to the low ratio of graphene and low diffraction intensity of graphene. The morphology of AIZS nanoparticles and AIZS-rGO nanocomposites were observed using transmission electron microscopy (TEM). A low magnification TEM image of the AIZS nanospheres ($Ag_{0.04}In_{0.23}ZnS_{1.365}$) were showed in Figure. 1B, it can be seen that big AIZS clusters with size of 100 nm was composed of small AIZS nanocrystal. Different ratio of AIZS nanoparticles($Ag_{0.01}In_{0.23}ZnS_{1.35}$,$Ag_{0.02}In_{0.23}ZnS_{1.355}$,$Ag_{0.05}In_{0.23}ZnS_{1.37}$) were prepared, and the shape of AIZS nanoparticles did not changed much (S_Figure 1, S_Figure 2A). Figure. 1C exhibited that nearly all the AIZS nanoparticles were grown on the graphene nanosheets to form as nanocomposites successfully, which may be due to the introduced rGO could provide an ideal platform for its nucleation of AIZS nanoparticles and improve the crystallinity of AIZS nanoparticles.[23] Moreover, as the size of the AIZS clusters was about 100 nm, which allowed photogenerated charge carriers moving rapidly to the surface to participate in the photocatalytic reaction. The lattice fringes of the composites were clearly observed by high resolution TEM（HRTEM）, as shown in Figure. 1D, it suggested that the AIZS nanoparticles were well crystallized. High-resolution TEM further revealed the crystalline characteristic of the AIZS-rGO composites, showing that the lattice fringes of individual AIZS clusters were 0.31 nm (111) and layered graphene (Figure 1D inset, S_Figure 2B).

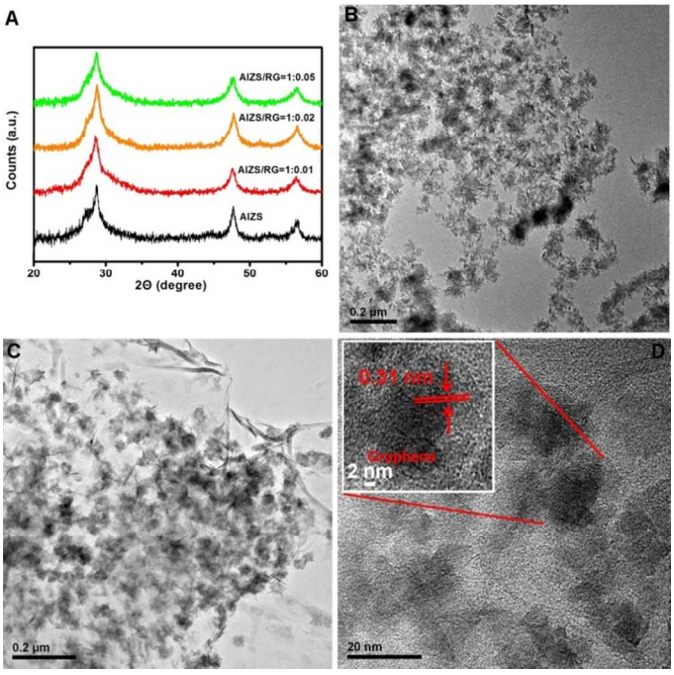

Figure. 1 (A) XRD patterns of AIZS-rGO nanocomposites with different ratio, (B) Low-resolution TEM image of $Ag_{0.04}In_{0.23}ZnS_{1.365}$ nanoparticles, (C) Low-resolution TEM image and (D) high-resolution TEM image of AIZS-rGO nanocomposites (inset is the magnified part of D).

The band edge absorption of AIZS nanoparticles played a crucial role on affecting the photocatalytic performances of photocatalysts. The UV-visible absorption spectra of AIZS nanoparticles with different rGO contents are shown in Figure. 2. The samples prepared with different weight ratios of rGO to AIZS, i. e. 0.01%, 0.02% and 0.05% were labelled as AG1, AG2 and AG5, respectively. The presence of different amounts of rGO would affect the optical property of light absorption for the AIZS-rGO composites significantly. The pure AIZS nanoparticles sample (red line) with an intense absorption edge of 460 nm. Compared with pure AIZS nanoparticles, the band absorption of AG1, AG2 and AG5 were systematically red shifted with increased amounts of rGO. At the same time, the color of the as-prepared AIZS nanoparticles and AIZS-rGO composites were changed to olive from yellow, and the color became deeper with increasing rGO. This phenomenon could be attributed to the chemical bonding between AIZS nanoparticles and the specific sites of carbon,[24] It could have a higher photocatalytic activity because the light absorption intensity of the AIZS-rGO composites was stronger than bare AIZS nanoparticles.[25-27]

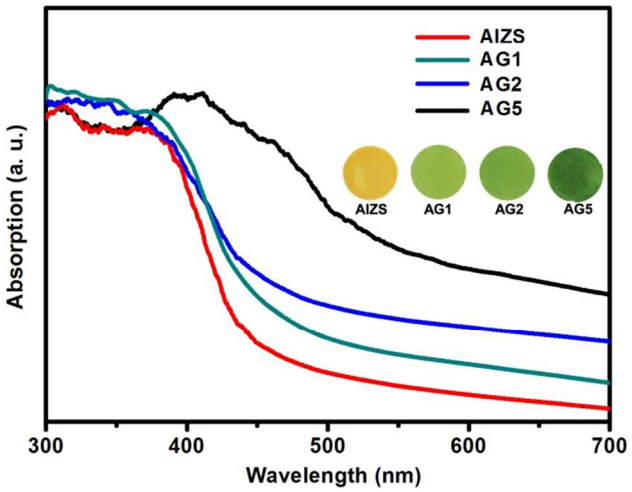

Figure. 2 UV-visible absorption spectra of AIZS nanocomposites with variable rGO content.

To explore the specific surface area and pore-size distribution of the as-prepared AIZS-rGO nanocomposites, Brunauer-Emmett-Teller (BET) gas-sorption measurement was employed to analyse those two factors, which would improve the catalytic performance greatly. Figure.3 is nitrogen adsorption-desorption isotherms and the corresponding pore size distribution curves of AIZS-rGO nanocompositions. From the Figure. 3A, it was observed that the hysteresis loop of the N_2 sorption isotherm for AIZS-rGO could be classified as type IV (according to IUPAC classification) at a relative pressure range between 0.5 and 0.9,[28] which indicated the presence of mesoporous (2-50 nm). Furthermore, the isotherm showed no limited adsorption at relative pressure (P/P_0>0.9) that revealing the extensive of large mesopores and micropores,[29] which probably due to the irregular assembly of nanoparticles in the nanocomposites.[25] In addition, the mean pore-size of AIZS-rGO nanocomposites was exhibited approximately 2-6 nm with narrow pore size distribution as revealed in Figure. 3B, further confirming the presence of mesopores and macropores,[29] which were caused by both porous AIZS nanospheres and rGO sheets. It was measured that the BET surface area of the as-prepared AIZS-rGO samples gradually expanded with increasing graphene content, the corresponding value of the samples increases up to 11.5056 $m^2 g^{-1}$ (from 70.3424 to 81.8480 $m^2 g^{-1}$), which was mainly due to the graphene-doping density was much lower than AIZS nanospheres. As the reason of the large surface area of the AIZS-rGO nanocomposites, it could provide more activity sites for reaction and facilitate more effective charge carrier transportation, and thus achieve high photocatalystic hydrogen production rate under visible light irradiation.[30]

In order to analyse the surface chemical states and the valence of AIZS nanospheres, X-ray photoelectron spectroscopy (XPS) was required to analyse AIZS nanospheres in the AG2 nanocomposites. As shown in Figure. 4A, the binding energies for Ag $3d_{5/2}$ and Ag $3d_{3/2}$ were 367.0 eV and 373.5 eV. It was observed that the In 3d core split into $3d_{5/2}$ (444.5 eV) and $3d_{3/2}$ (373.5 eV) peaks (Figure. 4B). The XPS spectrum of Zn 2p from AG2 was showed in Figure 4C, the peaks for Zn $2p_{3/2}$ and $2p_{1/2}$ located at 1022 eV and 1044 eV. From Figure 4D， it could be realized that the S 2p peaks were 161.3 and 162.2 eV. All of the above measurement results showed that the valence of the elements Ag, In, Zn and S were 1^+, 3^+, 2^+ and 2^-, respectively, which were in agreement with the reported date in the literature.[31,32]

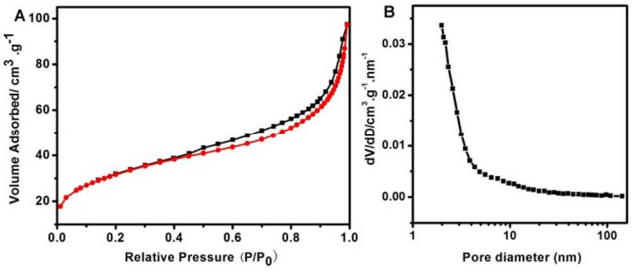

Figure. 3 Nitrogen adsorption-desorption isotherms (A) and corresponding pore size distribution curves (B) of AIZS-rGO nanocomposites.

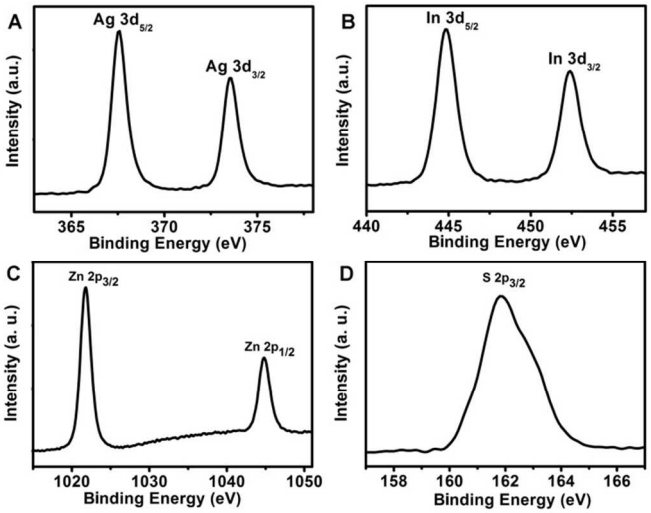

Figure. 4 XPS data from the surface of the AIZS nanoparticles in AG2 composites: (A) the XPS spectrum of Ag 3d, (B) the XPS spectrum of In 3d, (C) the XPS spectrum of Zn 2p, (D) the XPS spectrum of S 2p.

Based on the analyses above, it was reasonable to expect that the as-obtained AIZS-rGO composites would be an ideal photocatalysts under visible-light irradiation. In order to measure and compare the photocatalytic hydrogen production activities of aforementioned samples, 1.2 mol L^{-1} Na_2SO_3 and 0.7 mol L^{-1} Na_2S as sacrificial agents were used in aqueous solution, and the reaction system was evacuated after each run.

The comparison of the visible-light photocatalytic hydrogen production rates pure AIZS including $Ag_{0.01}In_{0.23}ZnS_{1.35}$, $Ag_{0.02}In_{0.23}ZnS_{1.355}$,$Ag_{0.04}In_{0.23}ZnS_{1.365}$ and $Ag_{0.05}In_{0.23}ZnS_{1.37}$ nanoparticles were estimated, and the best one of $Ag_{0.04}In_{0.23}ZnS_{1.365}$ nanoparticles was employed to prepare AIZS-rGO composites (S_Figure 3). The further hydrogen evolution study of the rGO, pure AIZS, AG1, AG2 and AG5 samples are shown in Figure. 5. The H_2-production activities of rGO and the pure AIZS nanospheres were measured for reference, it was observed that hydrogen was not detected when pure rGO was used alone as the photocatalyst, while pure AIZS nanospheres showed low photocatalytic H_2 production activities (0.951 mmol h^{-1} g^{-1}), which mainly owed to the nanoparticles introducing many recombination sites for conduction band (CB) electrons and valence band (VB) holes. Interestingly, with the small existing of graphene (0.01 wt %), the H_2 rate evolution of the sample of AG1 was slightly enhanced to 1.755 mmol h^{-1} g^{-1}, when the graphene further increase to 0.02 wt%, the rate of H_2 revolution reached 1.871 mmol h^{-1} g^{-1}, which was about 2 times of pure AIZS nanopaticles as photocatalyst. Normally, the photocatalytic reaction of AIZS nanoparticles was low because these charge carriers recombined quickly and only a fraction of electrons and holes participated. However, for the composite structure of AIZS-rGO nanocomposites, it could provide great numbers of photocatalytic active sites and adsorb more photons and reactants, which is the reason for the superior photocatalytic H_2 production activity to pure AIZS nanoparticles. On the contrary, an obvious degradation about the activity of hydrogen evolution when graphene-doping further increased to 0.05 wt % was observed, it was demonstrated that there was an optimal loading amount of graphene on the hydrogen production efficiency. This can be explained that the excessive loading of graphene may increase the opacity and block the visible light through the reaction solution, and similar phenomenon has been observed in other systems.[33-35]

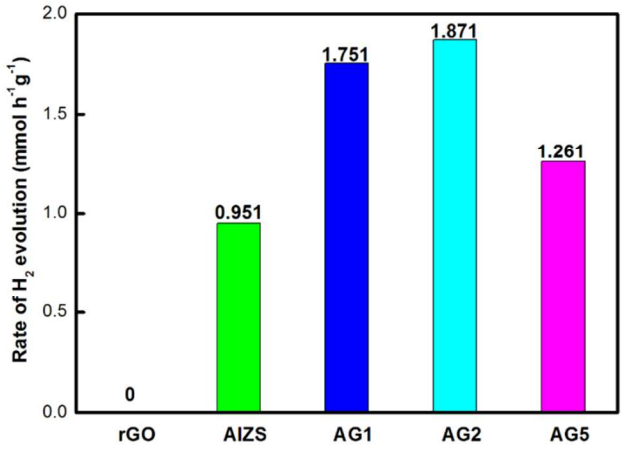

Figure. 5 Comparison of H_2 evolution rates of different samples under visible light irradiation in the mixed aqueous solution containing 1.2 mol L^{-1} Na_2SO_3 and 0.7 mol L^{-1} Na_2S as sacrificial agents, An 800 W Xe–Hg lamp was used as the light source.

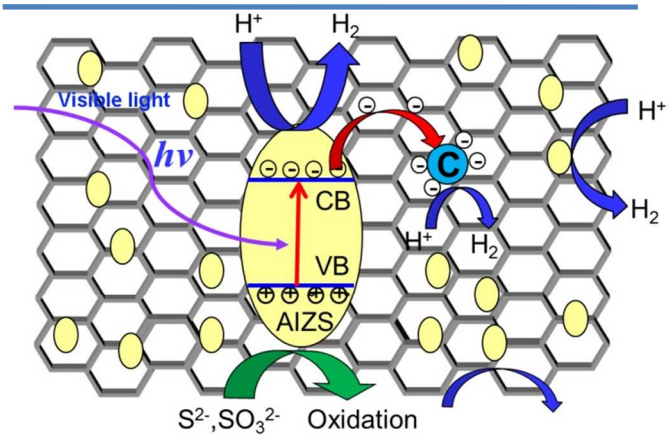

Scheme. 1 Schematic diagram of the electron transfer and hydrogen evolution in AIZS-rGO Photocatalyst.

During the process of reaction (Scheme. 1), the electrons (e^-) of AIZS nanoparticles were excited from the VB to the CB, thereby under visible light irradiation (λ>420 nm), creating holes in the VB and forming electron-hole pairs. The CB electrons of AIZS can reduce H^+ to produce H_2 and the holes accumulate at the VB of AIZS can react with S^{2-}/SO_3^{2-} solution.[36] On one side, some electrons in the VB were used to reducing H^+ that existed at round of the surface of AIZS nanospheres into H_2 directly. And on the other side, as the formation of chemically bond between AIZS nanoparticles and graphene, some photogenerated electrons could be transferred to the carbon atoms on the graphene nanosheets, thus facilitating the separation of photogenerated carriers and lengthening the lifetime of charge carriers, and reaction with H^+ to produce H_2. The mainly reactions during the hydrogen evolution production using AIZS-rGO composites as photocatalysts can be represented by the following equation (1)-(6):[37]

$$\text{AIZS} - \text{rGO} \xrightarrow{h\nu} \text{rGO}\ (e^-) + \text{AIZS}\ (h^+) \quad (1)$$

$$\text{rGO}\ (2e^-) + 2H^+ \rightarrow \text{rGO} + H_2 \quad (2)$$

$$\text{AIZS}\ (h^+) + H_2O + SO_3^{2-} \rightarrow \text{AIZS} + SO_4^{2-} + H^+ \quad (3)$$

$$\text{AIZS}\ (2h^+) + 2S^{2-} \rightarrow S_2^{2-} + \text{AIZS} \quad (4)$$

$$S_2^{2-} + SO_3^{2-} \rightarrow S_2O_3^{2-} + S^{2-} \quad (5)$$

$$\text{AIZS}\ (h^+) + SO_3^{2-} + S^{2-} \rightarrow S_2O_3^{2-} + \text{AIZS} \quad (6)$$

The Na_2SO_3 and Na_2S solution in this process play a key role in improving the photocatalytic H_2 production activity of AIZS-rGO nanocomposites, it has been proved that there was no H_2 can be detected when the solution was replaced by the frequently used sacrificial agent methanol.[38] In summary, the AIZS-rGO composites have several advantages, including an increase in the number of active adsorption sites and photocatalytic reaction centers, improvement of interfacial charge transfer and suppression of charge recombination, all of

these strongly suggest that the graphene doped in AIZS can enhance the hydrogen photocatalytic activity.

Conclusions

In summary, nanocomposites of AIZS-rGO have been synthesized successfully by a simple, convenient and low-cost hydrothermal method and can be used for visible-light-driven photocatalytic hydrogen evolution. It also has been proved as a new pathway to synthesize novel graphene-based photocatalystic materials. The result showed that the optimal graphene loading content was measured to be about 0.02 wt% and the corresponding H_2-production rate was 1.871mmol$h^{-1}g^{-1}$. This high and efficient photocatalytic activity for hydrogen production of AIZS-rGO composites mainly attributed to two factors: the presence of mesoporous structure with large specific surface area and the doping graphene would enhance the charge separation and transfer. Moreover, this work also showed the graphene-based materials have tremendous potential applications in solar energy conversion.

Acknowledgement

This work is supported by initial funding of Hundred Young Talents Plan at Chongqing University (0210001104430)， The Project-sponsored by SRF for ROCS, SEM (0210002409003)， the Fundamental Research Funds for the Central Universities， (0210005202042), the Fundamental Research Funds for the Central Universities (0210005202057).

Notes and references

[1] *Key Laboratory of Optoelectronic Technology and Systems of the Education Ministry of China, College of Optoelectronic Engineering, Chongqing University, Chongqing 400044, China*
[2] *College of Power Engineering, Chongqing University, China*
[3] *College of Materials Science and Engineering, Chongqing University, China*
[4]*Department of Materials Science & Engineering, National University of Singapore, Singapore*

1 R. D. Cortright, R. R. Davda, J. A. Dumesic, *Nature*, 2002, **418**, 964-967.
2 Y. Zhang, Y. Tang, X. Liu, Z. Dong, H. H. Hng, Z. Chen, T. C. Sum, X. Chen, *Small,* 201**3**, **9**, 996-1002
3 X. Wang, C. Liow, A. Bisht, X. Liu, T. C. Sum, X. Chen, S. Li, *Adv. Mater.,* 2015, **27**, 2207-2214.
4 Z. Jiang, Y. Tang, Q. Tay, Y. Zhang, O. I. Malyi, D. Wang, J. Deng, Y. Lai, H. Zhou, X. Chen, Z. Dong, Z. Chen, *Adv. Ener. Mater.*, 2013, **3**, 1368–1380
5 Z. G. Zou, J. H. Ye, K. Sayama, H. Arakawa, *Nature*, 2001, **414**, 625-627.
6 A. Hochbaum, P. D. Yang, *Chem. Rev.*, 2010, **110**, 527-546.
7 X. B. Chen, S. H. Shen, L. J. Guo, S. Mao, *Chem. Rev.*, 2010, 6503-6570.
8 I. Tsuji, H. Kato, H. Kobayashi, M. Kudo, *A. J. Am. Chem. Soc.,* 2004, **126**, 13406-13413.
9 Y. Li, G. Chen, C. Zhou, J. Sun, *J. Chem. Commun*., 2009, **15**, 2020-2022.
10 Y. Li, G. Chen, Q. Wang, X. Wang, A. Zhou, Z. Shen, *Adv. Funct. Mater.*, 2010, **20**, 3390-3398.
11 I. Tsuji, H. Kato, H. Kobayashi, A. Kudo, *J. Phys. Chem. B* ,2005,**109**, 7323-7329.
12 I. Tsuji, H. Kato, H. Kobayashi, A. Kudo, *Chem. Mater.,* 2006, **18**, 1969-1975.
13 Z. Y. Shen, G. Chen, Q. Wang, Y. G. Yu, C. Zhou, Y. Wang, *Nanoscale*, 2012, **4**, 2010-2017.
14 K. S. Novoselov, A. K. Geim, S. V. Morozov, D. Jiang,Y. Zhang, S. V. Dubonos, I. V. Grigorieva , A. A. Firsov, *Science*, 2004, **306**, 666-669.
15 A. K. Geim, K. S. Novoselov, *Nat. Mater.*, 2007, **6**, 183-191..
16 M. J. Allen, V. C. Tung, R. B. Kaner, *Chem. Rev.*, 2010, **110**, 132-145.
17 A. K. Geim, *Science*, 2009, **324**, 1530-1534.
18 Q. J. Xiang, J. G. Yu, M. Jaroniec, *Chem. Soc. Rev.*, 2012, 41, 782-796.
19 Y. H. Li, Y. J. Sun, F. Dong, W. K. Ho, *J. Colloid Interface Sci*, 2014, **436**, 29-36.
20 Q. J. Xiang, D. Lang, T. T. Shen, F. Liu, *Appl. Catal. B- Environ*, 2015, **162**, 196-203.
21 X. Zhang, H. Li, X. Cui, Y. Lin, *J.Mater. Chem.*, 2010, **20**, 2801-2806.
22 X. G. Mei, J. Y. Ouyang, *Carbon*, 2011, **49**, 5389-5397.
23 S. Lee, K. Lee, W. D. Kim, S. Lee, D. J. Shin, D. C. Lee, *J. Phys. Chem. C*, 2014, **118**, 23627-23634.
24 Y. Zhang, Z. Tang, X. Fu, Y. Xu, *ACS Nano*, 2010, **4**, 7303-7314.
25 X. Tang, Q. Tay, Z. Chen, Y. Chen, G. Gohc, J. Xue, *J. Mater. Chem A*, 2013, **1**, 6359-6365.
26 J. Huang, Y. Wu, D. Wang, Y. Ma, Z. Yue, Y. Lu, M. Zhang, Z. Zhang, P. Yang, *ACS. App.Mater.Interfaces*, 2015, **7**, 3732 - 3741.
27 H. Zhang, X. Lv, Y. Li, Y. Wang, J. Li, *ACS Nano*, 2010, **4**, 380-386.
28 K. Sing, D. Everett, R. Haul, L. Moscou, R. Pierotti, J. Rouquerol , T. Siemieniewska, *Pure Appl. Chem.*, 1985, **57**, 603-619.
29 J. G. Yu, J. J. Fan, K. L. Lv, *Nanoscale*, 2010, **2**, 2144-2149.
30 N. Bao, L. Shen, T. Takata, K. Domen, *Chem. Mater.*, 2008, **20**, 110-117.
31 S. Shen, L. Zhao, L. Guo, *J. Phys. Chem. Solids*, 2008, **69** , 2426-2432.
32 S. Peng, S. Zhang, S. G. Mhaisalkara, S. Ramakrishna, *Chem. Phys.,* 2012, **14**, 8523 - 8529.
33 K. Li, B. Chai, T. Peng, J. Mao, L. Zan, *ACS Catal*. 2013, **3**, 170-177.
34 Q. Li, N. Zhang, Y. Yang, G. Wang, D. H. L. Ng, *Langmuir*, 2014, **30**, 8965-8972.
35 B. Weng, J. Wu, N. Zhang, Y. J. Xu, *Langmuir*, 2014, **30** 5574-5584.
36 J. Yu, B. Yang, B. Cheng, *Nanoscale*, 2012, **4**, 2670–2677.
37 X. B. Chen, S. H. Shen, L. J. Guo, S. S. Mao, *Chem. Rev.*, 2010, **110**, 6503-6570.
38 C. Zhou, Y. Zhao, T. Bian, L. Shang, H. Yu, L. Wu, C. Ho Tunga, T. Zhang, *Chem. Commun.,* 2013, **49**, 9872-9874.

